CrystEngComm

Accepted Manuscript

ROYAL SOCIETY OF CHEMISTRY

www.rsc.org/crystengcomm

CrystEngComm

ARTICLE

Nanostructured Copper Sulfides: Synthesis, Properties and Applications

Received 00th January 20xx,
Accepted 00th January 20xx

DOI: 10.1039/x0xx00000x

www.rsc.org/

Poulomi Roy[a]* and Suneel Kumar Srivastava[b]*

Among different metal chalcogenides, copper sulfides are extensively studied in past few years due to semiconducting and non-toxic nature, making their use in wide range of applications from energy to biomedical field. A series of stoichiometric composition of copper sulfides from Cu-rich, Cu_2S to Cu-deficient, CuS_2 exist with different crystal structures as well as phases resulting different unique properties. The suitable band gap values in the range of 1.2-1.5 eV and unique optoelectronic properties indicate the material photocatalytically active and exhibit excellent plasmonic behavior. The material is also known for promising thermoelectric properties converting waste heat into electricity through Seeback effect. Nanodimensional form of copper sulfides promotes their use to more advanced level tuning their properties with size of the materials. In view of this, present review article is focused on compositions, phases and crystal structures, different synthetic methodologies involved in fabrication of 0D, 1D and 2D nanostructured copper sulfides. Moreover, the recent advancements on their use in various applications will also be briefly discussed.

1. Introduction

Copper sulfides are known to be a very important *p*-type semiconductor due to its versatility, availability and low-toxic nature. It exists in different phases ranging from copper-rich (Cu_2S) to sulfur-rich (CuS), which exhibit wide variation of their direct/indirect band gaps.[1, 2] Further, plasmonic absorption is observed near IR region in non-stoichiometric copper sulfide due to generation of free charge carriers.[1, 3-7] The electrical conductivity of copper sulfides very much rely on its composition and decreases from copper-poor to copper-rich compositions.[8, 9] Naturally occurring covellite phase of CuS shows extraordinary superconductivity at 1.63 K.[10] Owing to wide variation in optical as well as electrical properties, copper sulfides find promising applications in the field of optoelectronic devices,[11, 12] photocatalysis,[13, 14] photovoltaic cells,[4, 15, 16] sensors,[16] battery electrodes[17, 18] and biomedical[19-21] fields. Recent investigations have shown that size reduction of CuS into nanoscale dimension further causes significant alteration in their physical and chemical properties due to quantum confinement effect.[1,22, 23] Therefore, considerable attention has been focused on the fabrication of nanostructured copper sulfides with different size, shape and morphology. A variety of physical[24] as well as chemical[25, 26] methods has also been employed in fabricating different nanodimensional 0, 1 and 2D copper sulfides. The manipulation of their property based on the requirement were achieved with controlled growth process attaining different shapes of nanostructured copper sulfides, such as, nanoparticles,[21, 27, 28] nanoplates,[29-31] hollow spheres,[11, 25] nanorods,[32-35] nanowires,[18, 36, 37] nanotubes,[38] nanosheets[13] etc. In this regard, 0D nanocrystals (quantum dot nanoparticles) with high surface area and active surface plasmon resonance are found to be very useful in optoelectronics and bioapplications.[7] On the other hand, anisotropic structures of CuS are more suitable in electronic devices with directional electronic transportation and their structural integrity.[18, 39] Further manipulation on their properties can be attempted by fabricating copper sulfide-based hybrid nanostructures with the combination of other materials exhibiting enhanced activity by manifold in many energy applications.[5, 40-43]

Tough, a large number of review articles/books regularly appeared on nanostructured metal chalcogenides,[22, 23, 44-47] contemporary work on copper sulfides are still not surveyed inspite of its versatility over compositions, phases, size, shape, morphologies. In view of this, present review article is focused on formation of different phases of nanodimensional copper sulfide in terms of their crystal structure and synthetic methods. Further, tunable optical, electrical, thermal properties of copper sulfides depending upon their size and shape have been reviewed followed by their applications in multifaceted fields. Finally, smart approaches combining copper sulfides in developing hybrid nanostructures/nano heterostructures and their effective application in energy as well as biomedical fields has also been compiled.

[a] Department of Chemistry,
Birla Institute of Technology Mesra, Ranchi 835215, Jharkhand, India.
Email: poulomiroy@yahoo.com
[b] Department of Chemistry,
Indian Institute of Technology Kharagpur, Kharagpur 721401, West Bengal, India.
Email: sunil111954@yahoo.co.uk

2. Compositions, Phases and Crystal Structures of Copper Sulfide

Copper sulfides exist in different phases ranging from copper-rich (Cu_2S) to sulfur-rich (CuS). Till now eight different forms of copper sulfide are identified – chalcocite (Cu_2S), djurleite ($Cu_{1.97}S$), digenite ($Cu_{1.80}S$), anilite ($Cu_{1.75}S$), geerite ($Cu_{1.60}S$), spionkopite ($Cu_{1.40}S$), yarrowite ($Cu_{1.12}S$), covellite ($Cu_{1.00}S$) and often represented as $Cu_{2-x}S$ with very small x values.[48, 49] Depending on the packing of sulfur in the lattice, crystal structure of these forms has been divided into three groups, namely cubic close packing (anilite and digenite), hexagonal close packing (djurleite and chalcocite) and combination of hexagonal close packing and covalent bonding of the sulfur atoms (covelline).[48] However, crystal structures of yarrowite, spionkopite and geerite are still not determined. Furthermore, a phase transition on changing temperature has also been observed, e.g., chalcocite Cu_2S exhibit monoclinic phase (low-chalcocite) at a temperature below 104 ºC, which changes to hexagonal phase (high-chalcocite) between 104 and 436 ºC and transform further to cubic phase (cubic-chalcocite) above 436 ºC.[50, 51] All the phases follow different synthesis methods and properties making them extremely useful in most specific applications. Wei and his coworkers[50] calculated heat of formation (ΔH) and noted anilite ($Cu_{1.75}S$) as one of the most stable form of copper sulfide. Figure 1 shows the crystal structures of some selective forms of copper sulfides. All these forms of copper sulfides are *p*-type semiconductor due to the presence of Cu-vacancies in the lattice. The band gap values of copper sulfides varies with stoichiometry in $Cu_{2-x}S$ and increases with copper deficiency 'x' as evident from band gap values in Cu_2S (1.1–1.4 eV) and $Cu_{1.8}S$ (1.5 eV) and CuS (~2.0 eV).[1, 4] Therefore, compositional control of copper sulfides is the effective way in tuning their optoelectronic properties as per the requirement (see detailed discussion in Section 4.1).

Several investigations are reported on stoichiometric $Cu_{2-x}S$ nanocrystals for possible phase transition.[1, 7, 32, 49, 51, 52] Cassaignon and his coworkers[53] investigated influence of composition on the copper diffusion in copper sulfide ($Cu_{2-x}S$) with the help of impedance spectroscopy. The study was carried out at the $Cu_{2-x}S$/electrolyte interface in a galvanic cell $Cu|Cu^{2+}|Cu_{2-x}S$ at different potentials and composition modification was observed at the interface. Such change in composition was attributed to the Cu diffusion through the vacancies in the lattice on imposing the different potentials. Xie et al.[49] synthesized series of copper sulfide nanocrystals by solution-based method with its compositions varying from $Cu_{1.1}S$ to Cu_2S by incorporating Cu(I) in the lattice of starting material $Cu_{1.1}S$ and investigated its optical properties. Burda and his group[1] successfully synthesized $Cu_{2-x}S$ nanocrystal of compositions ranging from CuS (covellite) to $Cu_{1.97}S$ (djurleite) by varying reduction potential in the sonoelectrochemical method, adjusting the pH value in the hydrothermal method and by choosing different precursor pretreatments in the solventless thermolysis approach. Further, copper deficiency in the $Cu_{2-x}S$ nanocrystals exhibited localized surface plasmon resonance and effective plasmonic behavior in near-IR region.[4-7] Such special properties enable these materials to used in various photoelectrochemical and energy applications, which will be discussed later.

Poulomi Roy *received her M.Sc. degree in Chemistry from Vidyasagar University, India in 2002 and obtained her PhD on Inorganic Nanomaterials from Indian Institute of Technology Kharagpur, India in 2007. She spent 2008-2011 at Friedrich Alexander-Universität Erlangen-Nürnberg, Germany as a postdoctoral research fellow, where she worked on the development of self-organized TiO_2-based nanostructures and their various applications. Currently, she is working as an Assistant Professor at Birla Institute of Technology Mesra, India. Her current research interests include the synthesis of semiconductor nanomaterials and their applications in energy conversion and storage devices.*

Suneel Kumar Srivastava *was born in 1954 in Ismilepur (Sitapur), Uttar Pradesh. He received his M.Sc. degree in Inorganic Chemistry from Lucknow University, Lucknow. Subsequently, he completed his post graduate diploma in 'High pressure technology and technical gas reactions' and Ph.D in the field of 'Solid state chemistry' from Indian Institute of Technology, Kharagpur in 1979 and 1984, respectively. He also carried out his post-doctoral work as a DAAD Fellow in Technical University, Karlsruhe (1988–89, 2003, 2006), University of Siegen (1994, 1999), Technical University, Munchen (2009) and Leibniz Institute of Polymer Research, Dresden (2013) Germany, and University of Nantes, France (2003, 2007). He is currently Professor in the Department of Chemistry, Indian Institute of Technology, Kharagpur. His research interests are in the field zero, one and two dimensional semiconducting and magnetic nanomaterials for their application in energy and environments, polymer and polymer blends and their structure-property relationships. He has guided 14 Ph.D and published about 125 research papers in referred journals.*

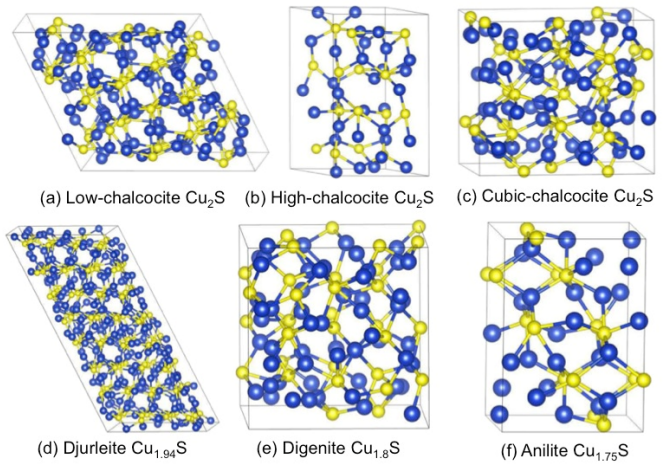

Figure 1: Crystal structures of (a) the low-chalcocite (monoclinic), (b) high-chalcocite (hexagonal), (c) cubic-chalcocite (cubic), (d) djurleite, (e) digenite, and (f) anilite. Reprinted with permission from ref. 50. Copyright 2012 American Institute of Physics.

3. Synthetic Strategies of Nanostructured Copper sulfides

A variety of synthetic strategies have been employed to prepare nanodimensional copper sulfides of different compositions and phases. According to available literature, composition of copper sulfides could be controlled by changing the molar ratios of Cu-precursor and S-precursor during the synthesis process. In addition, the control over the morphology or shape, size of the nanostructured copper sulfides with tunable properties is executed by changing reaction parameters. In this section, we will discuss different methodologies and their mechanisms involved in the fabricating nanodimensional copper sulfides of various morphology.

3.1 Hydrothermal / Solvothermal Method

Hydrothermal/solvothermal methods remain even till date as one of most commonly used method in synthesizing nanomaterials. The technique enables increase in the solubility of reactants in solvent and speed up the chemical reaction attaining quick supersaturation under high temperature and pressure. Accordingly, synthesis of copper sulfides were successfully achieved in the form of nanoparticles, nanorods, nanowires or nanotubes by this approach.[31, 54-61] The application of stabilizing/capping agents has also been extensively employed in order to stabilize narrow size distribution in 0D and specific high energy surfaces in 1D and 2D nanostructures of copper sulfide. Du et al.[31] synthesized single-crystalline, hexagonal covellite (CuS) nanoplatelets (Dia: 26 nm, Thickness: 8 nm) by solvothermal method in presence of hexadecylamine and toluene as a capping agent and solvent, respectively. These nanoplatelets exhibit tendency to self-assemble into pillar-like, raft-like and stratiform nanostructures. Though, size of the nanoplatelets could be tuned by varying the reaction temperature, self-assembled stacking was mostly controlled by the capping agent and van der Waals attraction.[31] An interesting approach was attempted by Zhuang et al.[62] on bottom-up self assemblies of Cu_2S nanocrystals into a superlattice at water-oil interface in an autoclave. In this case, dodecanethiol was used as oil phase as well as the capping agent. It is believed that the size as well as shape of nanocrystals can be engineered by changing the concentration of Cu^{2+} and dodecanthiol, whereas the self-assembly of nanocrystals can be controlled by adjusting the dipole-dipole and van der Waals interactions. In addition, polymers were also often used as a capping agent to prepare copper sulfide superstructures under hydrothermal conditions.[13, 14, 20, 58, 63, 64] Zhang et al.[63] synthesized CuS nanotubes by solvothermal process in a microemulsion system consisting of oleic acid, water and poly(vinylpyrrolidone). Jia and his co-workers[54] reported facile synthesis of hexagonal bifrustum-shaped copper sulfide (CuS) nanocrystals via hydrothermal method assisted by tetradecylamine. Different non-stoichiometric compositions of copper sulfides: CuS (particle), mixture of Cu_7S_4–CuS (hexagonal plate) and Cu_9S_5 (octahedron nanocrystals) were fabricated by solvothermal method simply by varying the ratios of Cu and S precursors.[55] The formation of such different morphologies of copper sulfides was attributed to the oriented-attachment mechanism of copper sulfides. Zhang et al.[56] synthesized CuS nanocrystals of spherical nanoflowers, doughnut-shaped nanospheres, and dense nanosphere shapes via solvothermal method. Interestingly, different morphologies were obtained under the same reaction conditions but changing the S-precursors, Na_2S, $Na_2S_2O_3$ or $CS(NH_2)_2$ led to the formation of different Cu-complexes, $[Cu(S_2O_3)(H_2O)_2]$, $[Cu(S_2O_3)_2]^{2-}$ or $[Cu\{CS(NH_2)_2\}_n]Cl$ and account for the formation of their variable morphology. Different nanostructures of CuS were prepared by varying the ratio of water : ethylene glycol as solvent, precursors ratios, reaction temperature and duration under hydrothermal treatment in the temperature range 150-250 ºC.[59] Further, addition of CTAB as surfactant reduced agglomeration to form well-dispersed nanocrystals. The complex formation phenomena with Cu(II) and S-precursors or use of single source precursor and their decomposition during the hydrothermal or solvothermal method plays very important role for the growth of nanocrystals leading to various morphologies of copper sulfides.[30, 56, 57, 59-61] Lou and his co-workers[30] synthesized high-quality, uniform copper sulfides (CuS and Cu_9S_5) in the form of faceted nanocrystals and triangular nanoplates by the decomposition of copper dialkyldithiophosphates via solvothermal method. The size of such nanocrystals were adjusted from 8 – 16 nm varying the carbon number of the substitute alkyl and reaction temperature in presence of oleylamine as a stabilizing agent. Our group subjected Cu-dithiooxamide complex as a single source precursor in an autoclave at 120 ºC.[61] It was noted that several µm long CuS nanowires with 70 nm of diameter were obtained under hydrothermal condition, whereas use of ethylenediamine or toluene instead of water leads to the formation of CuS nanoparticles only. In another attempt, our group studied the growth of flower-like morphology of copper sulfides from nanorods with different compositions by solvothermal method using ethylenediamine as solvent.[65]

Furthermore, various morphologies as well as stoichiometries have also been fabricated by using different chelating and nonchelating solvents in solvothermal method as reported elsewhere.[66] Zhao and his co-workers[26] carried out organic amine-assisted hydrothermal method to assemble digenite phase copper sulfide nanoparticles into various shapes - nanowires, nanotubes, and nanovesicles using triethylenediamine, tramethylethylenediamine, di-n-butylamine, respectively as linking agent at low temperature range 90-110 ºC.

A number of attempts have also been made in fabricating nanocomposites of copper sulfide and carbon nanotubes by hydrothermal method.[16, 67-70] These nanocomposites exhibit very promising properties in the field of solar cells and sensors. Park and his co-workers[16] fabricated Cu_2S nanocrystals anchored on the surface of multi-walled carbon nanotubes (MWCNT) via solvothermal process using oleylamine as solvent. They also manipulated the size of Cu_2S nanocrystals by simply changing the molar ratio of Cu- and S-precursors. A similar work has also been reported on CuS nanoparticles on MWCNT via hydrothermal process.[70] Copper sulfide-core/carbon-sheath cables were prepared via hydrothermal method in presence of β–cyclodextrin acted as both ligand and carbon source of the sheath.[67] Another interesting strategy in fabricating ultrafine CuS nanoneedle arrays on a CNT backbones involved the combination of template-engaged conversion route followed by hydrothermal treatment.[68] In this approach, silica coated CNTs (CNT@SiO_2) was first introduced as the substrate for the growth of copper silicate (CuSilicate) nanoneedles to form 1D CNT@SiO2@CuSilicate core–shell. Subsequent hydrothermal treatment converted it into CuS nanoneedles@CNT accompanied by selective etching of SiO_2 by OH^- ions.

3.2 Hot-injection Method

Other than hydrothermal/solvothermal methods, one-pot hot-injection method is another frequently used technique to synthesize monodispersed, high-quality copper sulfide nanocrystals from the mixture of organic solvents and appropriate surfactants in a standard Schlenk set-up.[7, 49, 71, 72] The mechanism relies on the sudden addition of cold reactants (room temperature) into hot solvent leading to sudden burst of nucleation and subsequent growth of nuclei in presence of surfactant under optimum reaction condition.[73] Ever since Bawendi and his group[74] developed this method for monodispersed Cd-chalcogenides, it has been further extended to other metal chalcogenides including copper sulfides.

Xie and his co-workers[71] successfully synthesized covellite CuS nanodisks by this approach. According to this, fast addition of S (sulphur)/OLAM (oleylamine) solution to the pre-heated (180 ºC) mixture of CuCl/OLAM/OLAC/ODE (copper chloride/oleylamine/oleic acid/1-octadecene) followed by a short annealing period resulting the formation of monodispersed hexagonal shaped CuS nanocrystals. Depending upon the binary OLAC/OLAM surfactant ratio, size

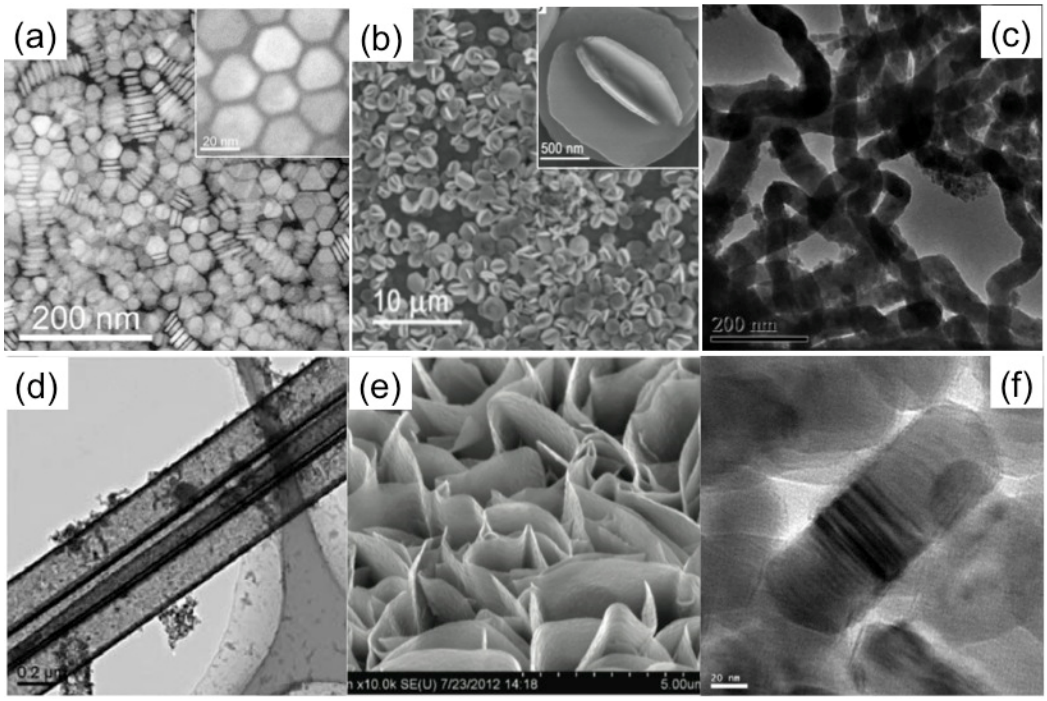

Figure 2: SEM and TEM images of different nanostructures of copper sulfides prepared by various methods: (a) Monodispersed CuS nanodisks by hot-injection method. Reprinted with permission from ref. 71. Copyright 2013 American Chemical Society. (b) Flower-Like CuS Superstructures by controlled hydrothermal method. Reprinted with permission from ref. 20. Copyright 2011 John Wiley and Sons. (c) CuS nanowires obtained under hydrothermal method. Reprinted with permission from ref. 61. Copyright 2006 American Chemical Society. (d) CuS nanotubes prepared from a single source precursor under microwave irradiation. Reprinted with permission from ref. 85. Copyright 2011 Royal Society of Chemistry. (e) Copper sulfide nanowalls vertically grown on to the substrate by electrochemical anodization of copper foil in aqueous Na_2S electrolyte at 1.5 V at room temperature. Reprinted with permission from ref. 86. Copyright 2014 Royal Society of Chemistry. (f) CuS nanorods with twinned structure synthesized by *in-situ* source template interface reaction method. Reprinted with permission from ref. 95. Copyright 2008 American Chemical Society.

of nanocrystals varied from 10 nm to 28 nm. Non-stoichiometric $Cu_{1.8}S$ nanocrystals (6-20 nm) were also prepared by the same technique as reported by Liu et al.[7] An *in situ* phase transformation from rhombohedral $Cu_{1.8}S$ nanocrystal to hexagonal CuS clusters was observed due to OLAM-assisted oxidation process by keeping the colloidal solution for few days. Ghezelbash and Korgel[75] synthesized hexagonal CuS (covellite)/ rhombohedral $Cu_{1.8}S$ (digenite) nanocrystals (Dia: 10-15 nm) in a dichlorobenzene-solvated medium by varying OLAC/OLAM molar ratios. The combination of 1-dodecanethiol and oleic acid as solvent and their variable ratios at a reaction temperature range 200-220 ºC often produced non-stoichiometric monodispersed $Cu_{2-x}S$ nanoparticles (Dia: 2-10 nm).[15, 72, 76] The formation of such non-stoichiometric $Cu_{2-x}S$ nanoparticles lies upon the reducing ability of dodecanethiol versus oleic acid and the growth of particles often accelerated to unusual faceted shape in presence of oleic acid.[76] Kruszynska et al.[32] observed that reaction temperature plays a very important role in determining size and shape of copper sulfide nanocrystals. Accordingly, they successfully prepared $Cu_{2-x}S$ nanocrystals to nanorods with adjustable length by careful choice of S-precursors (*1*-dodecanethiol/*tert*-dodecanethiol or *t*-DDT) followed by adjusting the nucleation temperature and copper monomer concentration. It is noted that *t*-DDT at high temperature promotes the reactivity of (100) surfaces of djurleite particles and favors the one-dimensional growth in to CuS nanorods. Nørby and his coworkers[51] reported the formation, growth, and phase transition of colloidal $Cu_{2-x}S$ nanocrystals in presence of DDT as a reducing agent as well as a size and shape controller. It is also observed that particle size of $Cu_{2-x}S$ nanocrystals decreases with increasing the concentration of DDT.[52] However, contradicting findings are also reported on increasing size of Cu_2S nanocrystals with DDT content, temperature, and reaction time.[77] The nanocrystal of *β*-Cu_2S (hexagonal) with narrow size distribution (2-10 nm) has been prepared in a media containing 1:2:1 molar ratio of $[Cu^+]$/[TGA] (thioglycolic acid)/[TAA] (thioacetamide).[78] It is believed that TGA stabilizes the nanoparticles as in absence of TGA results in the self-assembly of nanoparticles to nanoribbons through the epitaxial matching of the particle surfaces.

The technique has also been extensively used in fabricating controlled shape and size nano heterostructures of copper sulfides. Gao and his co-workers[42, 79] prepared $Cu_{1.94}S$-M_xS_y (M = In, Zn) heterostructured nanorods by multi-step injection of $M(acac)_y$-dodecanethiol stock solutions into a hot $Cu(acac)_2$-dodecanethiol reaction system. In either case, heteronanostructures of $Cu_{1.94}S$-In_2S_3[79] and $Cu_{1.94}S$-ZnS[42] were achieved by the epitaxial growth of In_2S_3 and ZnS on to the $Cu_{1.94}S$ and seed were controlled by injection time as well as molar ratio of $In(acac)_3$: $Cu(acac)_2$ or $Zn(acac)_2$: $Cu(acac)_2$ respectively. Such seed-mediated growth results matchstick-like morphology of $Cu_{1.94}S$ as head and In_2S_3 and ZnS acting as tails. Further, a series of nanocrystals of Cu_2S–metal chalcogenides, including Cu_2S–ZnS, Cu_2S–CuInS, and Cu_2S–CuInZnS in the form of nanocrystals to nanorods were also prepared in octadecene-mediated medium containing DDT as capping agent.[41] In another two-step strategy, dimeric $Cu_{1.94}S$-ZnS nanoheterostructure were fabricated by dispersing $Cu_{1.94}S$ nanocrystals in OLAM under hot condition followed by injecting of Zn-oleate and dodecanethiol into this mixture.[80] The proposed mechanism involved the ion exchange reaction of Zn with Cu ions in $Cu_{1.94}S$ nanospheres embedding the ZnS crystal into the nanosphere followed by the directional growth of ZnS nanoslab on the embedded ZnS crystals. Further, complex structures of different $Cu_{1.94}S$-ZnS, $Cu_{1.94}S$-ZnS-$Cu_{1.94}S$, and $Cu_{1.94}S$-ZnS-$Cu_{1.94}S$-ZnS-$Cu_{1.94}S$ heteronanostructures with screw, dumbbell, and sandwich-like shapes were also fabricated by the one-pot colloidal route by varying the molar ratios of Cu- and Zn-precursors in oleylamine.[43]

3.3 Thermolysis

This method involved formation of copper sulfide nanostructures by thermal decomposition of Cu-S complex as single source precursors. The hot-injection method, as discussed earlier, could also be considered as the effective solvent-mediated thermolysis of Cu-S complex in presence of a capping agent. However, a number of solvent-less thermolysis process also produced different nanostructured copper sulfides. Korgel and his group[33, 81] fabricated Cu_2S nanocrystals from copper alkylthiolate single source precursor by solvent-less thermolysis at a temperature range 140-200 ºC. They used sodium octanoate as a capping agent during the preparation of thiolate precursor in organic medium to control the anisotropic growth of Cu_2S nanocrystals of different shapes, e.g, nanorods, nanodisks and nanoplatelets or their assemblies to form multilayer superlattices. Such oriented growth of Cu_2S depends on the differences in surface energy of (001) and (100), (110) facets. Chen et al[82] prepared Cu_2S nanowires of high aspect ratio by the thermolysis of Cu-thiolate polymer precursor. It is also inferred that aspect ratio of Cu_2S nanowires could be modified by alteration of polymeric chain length of precursor, controlling the viscosity of colloidal precursor. Solvent-mediated thermal decomposition of Cu-alkylthiophosphates at moderate reaction temperature range (120-200 ºC) led the formation of monodispersed CuS nanocrystals and triangular CuS nanoplates.[30] A number of reports are also available on direct thermal decomposition of Cu-S complex precursors, e.g., Cu-thiolate,[83] Cu-dithiooxamide[61] or Cu-alkyldithiocarbamate[84] complexes. It is anticipated that the size and shape of such nanocrystals entirely depends upon the crystal structures of the single source precursors. The decomposition of complex precursors under microwave irradiation by thermolysis has also been carried out to synthesize copper sulfide nanocrystals, which is discussed in detail in the next section 3.4.

3.4 Microwave Irradiation

Chemical synthesis under microwave irradiations in a frequency range 0.3 to 2.45 GHz remains comparatively one of the fastest strategies.[87] Under this microwave frequency range, electromagnetic energy is converted into thermal energy, which induces chemical reaction leading to the

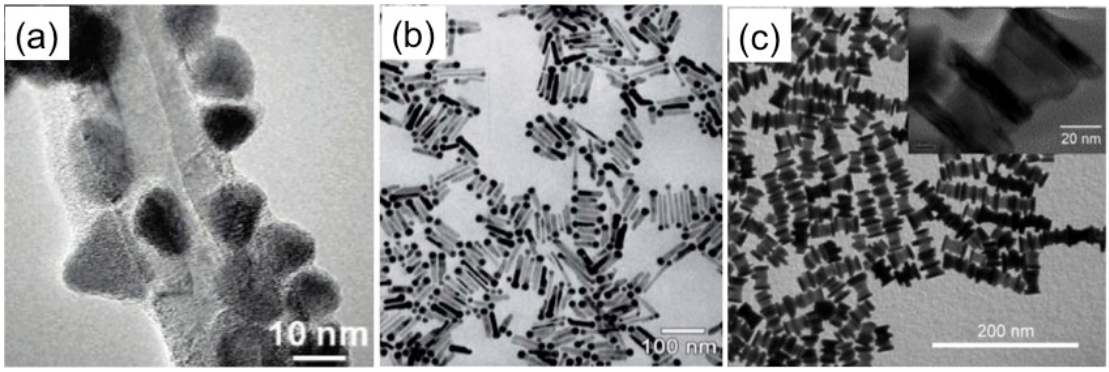

Figure 3. TEM images of copper sulfide – based hybrid nanostructures prepared by different techniques: (a) Cu_2S-MWCNT nanocomposites by solvothermal method. Reprinted with permission from ref. 16. Copyright 2007 American Chemical Society. (b) $Cu_{1.94}S$-ZnS nanoheterostructure fabricated by hot-injection method. Reprinted with permission from ref. 42. Copyright 2010 Royal Society of Chemistry. (c) $Cu_{1.94}S$-ZnS-$Cu_{1.94}S$-ZnS- $Cu_{1.94}S$ sandwich-like heteronanostructures by hot-injection method. Reprinted with permission from ref. 43. Copyright 2012 John Wiley and Sons.

synthesis of nanostructured materials. This approach has successfully been employed for rapid decomposition of single source precursor into CuS nanotubes in presence of diethanolamine as a solvent.[85] The diameter of several micrometer long CuS nanotubes further were tuned in the range of 150-500 nm by altering the reaction temperature, choice of solvent as well as use of surfactant. In another report, non-stoichiometric copper sulfide (Cu_9S_8) nanorods were prepared by decomposition of Cu-thioacetamide complex in sodium dodecyl sulfate aqueous solution under microwave irradiation.[34] Thongtem et al.[88] prepared CuS nanotubes in absence of any surfactant following the decomposition of Cu-thioacetamide complex by microwave-assisted solvothermal method. In addition, various hierarchical nanostructures of CuS were also prepared by simple mixing Cu-precursors and S-precursors in presence of EDTA as complexing agent or additives or surfactants under microwave irradiation.[89-91] The formation of stable Cu-EDTA complex in compared to the weak interaction among Cu^{2+} and surfactant lead to the formation of 3D flower-like morphology of CuS with oriented arrangement, which further undergo the 1D chain-like growth via self-assembly.[89]

3.5 Electrodeposition

Electrochemical deposition or anodization is another simple, low cost and high-throughput technique to fabricate copper sulfide nanostructure on to the substrate directly. Like, many other metal oxides, copper sulfide nanostructures are also grown on Cu-substrates or Cu-foil acting as anode and Ti-metal as cathode in the voltage range of 1.5 – 8 V in Na_2S aqueous solution.[86] Accordingly, Cu_2S and CuS nanorod and nanowall arrays were achieved by manipulating the voltage as well as the reaction temperature. Xu and his co-workers[92] successfully fabricated hierarchical CuS nanostructures by electrochemical deposition on to the conductive fluorine-doped tin oxide (FTO) - coated glass substrate at -1.05 V in a DMSO based electrolyte containing Cu-salt and S-powder and $NaNO_3$ as supporting electrolyte at 80 ºC. Further, CuS nanorods and nanowires were also deposited on to the conductive stainless-steel substrate by the similar technique at room temperature.[93, 94] It is also noted that diameter of nanowire could vary between 40-600 nm and their lengths up to 300 µm depending on the deposition duration.[94] Though, chemical method is very simple and efficient, very limited work has been reported even till now in fabricating copper sulfide nanostructures.

3.6 Others

In addition to above conventional methods, a number of strategies has also been utilized for fabrication of different copper sulfide nanostructures. *In situ* source-template-interface reaction (ISTIR) route is a simple wet chemical method to fabricate different nanostructures (nanoparticles and nanorods) of CuS in a controlled way.[95] The reaction mechanism lies at the interface of water-oil microemulsion solution, where CS_2 act as a sulphur source as well as oil phase and ethylenediamine was used as a complexing agent to control the release of free Cu^{2+} ions. The growth of nanostructures was simply controlled by changing the reaction temperature. Interestingly twinned structure was observed in the CuS nanorods at low reaction temperature due to insertion of stacking fault during slow reaction process. A most commonly accepted approach in preparation of copper sulfide nanotubes involved copper-thiourea complex $[Cu(tu)]Cl{\cdot}1/2H_2O]$ nanowire precursor as self-sacrificial template.[96-98] The complex itself act as a single source precursor for both Cu as well as S and the crystallization of CuS starts at the surface by the decomposition of thiourea. The subsequent dissolution of complex towards interior results the formation of porous CuS nanotubes. Similar approach has also been attempted by using Cu nanowires[99, 100] or its different complexes, such as, Cu-thioacetamide, $Cu(OH)_2$[101, 102] or $CuSn(OH)_6$[103] in the form of nanorods or nanowires as self-sacrificial template.

Syntheses of nanostructured hybrid materials of copper sulfide with carbonaceous materials (SWCNT, MWCNT etc.) has also been reported due to their potential applications. In most of the cases, these hybrid materials were prepared hydrothermally or solvothermally[16] (see Section 3.1) mixing acid-treated CNTs with Cu- and S-precursors. The successful anchoring of CuS nanoparticles on to the SWCNT surface were also carried out via functionalizing the SWCNT surface by oleylamine in toluene-based reaction medium.[104, 105]

Table 1: An overview of various synthetic methods to prepare different nanostructured copper sulphides.

No.	Sample	Methods	Capping agent	Dimension	Ref.
A.	**Zero-dimensional**				
1.	CuS nanoplatelets	Solvothermal	Hexadecylamine	Dia: 26 nm Thickness: 8 nm	31
2.	CuS hexagonal bifrustum nanocrystals	Hydrothermal	Tetradecylamine	Edge length: 50-70 nm L: 250 nm	54
3.	Pure CuS, a mixture of CuS–Cu_7S_4, and Cu_9S_5 nanocrystals	Solvothermal	--	Width: 500 nm – 1 µm Thickness: 50 nm	55
4.	CuS hexagonal nanoplates	Hydrothermal	--	Edge length: 1 µm Thickness: 100nm Crystallite size: 45 nm	57
5.	CuS and Cu_9S_5 triangular nanoplatlets	Solvothermal	OLAM	8 – 16 nm	30
6.	CuS nanodisks	Hot-injection method	OLAM/OLAC	10-28 nm	71
7.	$Cu_{1.8}S$ nanocrystals	Hot-injection method	OLAM/OLAC	6-20 nm	7
8.	CuS and $Cu_{1.8}S$ nanocrystals	Hot-injection method	OLAM/OLAC	10-15 nm	75
9.	$Cu_{2-x}S$ nanoparticles	Hot-injection method	1-DDT/OLAC	2-10 nm	72
10.	$Cu_{2-x}S$ nanocrystals	Hot-injection method	DDT	11-18 nm	51
11.	$Cu_{1.75}S$ nanoplates and Cu_2S nanoparticles	Hot-injection method	TOP or TBPT and DDT	20-90 nm	52
12.	β–Cu_2S nanoparticles	Hot-injection method	TGA	2-10 nm	78
13.	Cu_2S nanodisks	Thermolysis	-	8-27 nm	83
B.	**One-dimensional**				
14.	CuS nanowires	Hydrothermal		Dia: 70 nm L: several µm	61
15.	CuS nanowires	Hydrothermal	triethylenediamine	Dia: 120 nm L: 2 µm	26
16.	CuS nanotubes		tramethylethylenediamine	Dia: 40-200 nm L: 400 nm – 4 µm	
17.	CuS nanovesicles		di-n-butylamine	50-180 nm	
18.	CuS nanotubes	Solvothermal	OLAC, poly(vinylpyrrolidone)	Dia: 30-90 nm Thickness: 40-80 nm	63
19.	CuS nanorods	*In situ* source-template-interface reaction	ethylenediamine	Dia: 10 nm L: 100 nm	95
20.	$Cu_{2-x}S$ nanorods	Hot-injection method	*tert*-DDT	L: 15-100 nm	32
21.	Cu_2S nanorods, nanodisks and nanoplatelets	Solvent-less thermolysis	sodiumoctanoate	L: 12 nm W: 4 nm	33, 81
22.	Cu_9S_8nanorods	Microwave irradiation	sodium dodecyl sulfate	L: 30-60 nm Dia: 5-10 nm	34
23.	Elongated Cu_2S nanocrystals	Solvent-less thermolysis	DDT	L: 14 nm W: 9 nm	62
24.	Cu_2S nanowires	Solvent-less thermolysis	-	L: 0.1 µm – several µm W: 2-6 nm	82
25.	CuS nanotubes	Microwave irradiation	CTAB	L: several µm Dia: 150-500 nm	85
26.	CuS nanotubes	Microwave-assisted Solvothermal	--	L: 20 µm Dia: 300-600 nm	88
27.	CuS nanotubes	Self-sacrificial template	--	Dia: 100±30 nm L: 200±100 µm	96
28.	CuS nanowires	Electrodeposition	--	Dia: 60-400 nm L: 300 µm	94
29.	Cu_2S–ZnS, Cu_2S–CuInS, and	Hot-injection method	DDT	L: 26 nm	41

	Cu_2S–CuInZnS nanorods			W: 7-8 nm	
30.	$Cu_{1.94}S$-In_2S_3 nanorods	Hot-injection method	DDT	L: 45-55 nm W: 13-14 nm	79
31.	$Cu_{1.94}S$-ZnS nanorods	Hot-injection method	DDT	L: 30-40 nm W: 20 nm	42
32.	$Cu_{1.94}S$-ZnS nanoheterostructure	Hot-injection method	DDT	20-25 nm	80
33.	$Cu_{1.94}S$-ZnS-$Cu_{1.94}S$-ZnS-$Cu_{1.94}S$ sandwich-like heteronanostructure	Hot-injection method	DDT	20-50 nm.	43
C.	**Superstructures**				
34.	CuS Superstructure	Hydrothermal	poly(vinyl pyrrolidone)	Edge length: 500-800 nm Thickness: 50 nm	20
35.	CuS nanocrystals - nanoflowers, doughnut-shaped nanospheres, and dense nanospheres	Solvothermal	--	Diameter: few µm Flake thickness: few nm	56
36.	CuS ball-flowers	Hydrothermal	poly(vinyl pyrrolidone)	Dia: 1.8-2.4 µm	14
37.	$Cu_{2-x}S$ flowers	Solvothermal	Ethylenediamine	Few µm	65
38.	CuS nanosheet-based hierarchical microspheres	Solvothermal	poly(vinyl pyrrolidone)	2.3 µm	13
39.	Hierarchical CuS flower-like morphology	Microwave Irradiation	EDTA/NH3/CTAB/SDBS	Nanoplate thickness: 50 nm	89
40.	Cu_2S and CuS nanorod and nanowall arrays	Electrochemical Anodization	--	Width: 50 nm	86
41.	Hierarchical CuS Nanostructures	Electrochemical deposition	--	Dia: 500-700nm Film thickness: 500 nm	92
D.	**Nanocomposites**				
42.	Cu_2S nanocrystals on MWCNT	Solvothermal		NC dia: 4 nm	16
43.	CuS NP-MWCNT hybrid nanostructure	Hydrothermal	Na-dodecyl sulfate	NP dia: 150 nm	70
44.	CuS/C core/shealth nanocables	Hydrothermal	β–cyclodextrin	Dia: 2 µm L: several µm Thickness: 300-400 nm	67

TOP: trioctylphosphine; TBPT: tributylphosphite; DDT: Dodecanethiol; TGA: Thioglycolic acid; OLAM: oleylamine; OLAC: oleic acid; CTAB: hexadecyltrimethyl ammonium bromide; SDBS: sodium dodecylbenzenesulfonate

4. Properties of Nanostructured Copper Sulfides

4.1 Optical Properties

Owing to a variety of compositions, copper sulfide nanocrystals are considered to be promising material for their application in optoelectronic devices. Earlier, $Cu_{2-x}S$ was considered to be both direct as well as indirect band gap semiconductors due to the appearance of absorption peaks in UV-Vis and NIR.[4, 7, 32, 106, 107] Later on, Lukashev et al.[2] suggested the non-existence of indirect band gap in $Cu_{2-x}S$ as per their theoretical calculations irrespective of its different phases, differing from previous reports. In support of the calculations by Lukashev et al.[2], Burda and his co-workers[1] ruled out the existence of indirect band gap and stated the direct band gap of $Cu_{2-x}S$ is a function of x due to Moss-Burstein effect[108, 109] caused by copper deficiency. When x-values increase, the hole formation near the valence band leads the shifting of energy of the lowest occupied energy level and altering of band gap value of $Cu_{2-x}S$.[110] The nanocrystal size dependent bang gap values have also been well studied by several research groups.[71, 83, 110] As expected, $Cu_{2-x}S$ exhibit strong quantum confinement effect for its size < 10 nm showing blue shift in the absorption spectra compared to bulk structures.[1, 3] Further, size dependence shift in UV-Vis spectra of $Cu_{2-x}S$ nanocrystals is found to be more prominent than the compositional dependence due to the Moss-Burstein effect.[1, 3, 109] Based on findings reported by several groups, Figure 4(a-c) show band gap dependence of copper sulfides with composition, size and shape of nanocrystals. Alivisatos and his coworkers[110] observed a clear blue shift from 1.3 eV to 1.6 eV in the UV-Vis absorption spectra, as the size of $Cu_{2-x}S$ nanocrystals decreases from 5.9 nm to 2.9 nm. In another report, comparatively larger nanodisks of Cu_2S with diameter 21.7 nm and 26.0 nm, synthesized by thermolysis of a single source precursor showed blue shift in their UV-Vis absorption spectra.[83]

In addition to the absorption band in the UV-Vis range, a broad band in NIR is also observed in $Cu_{2-x}S$ nanocrystals. Though, earlier it was misinterpreted as the indirect band

nature, later it was confirmed that such band in NIR is due to the plasmonic behavior of $Cu_{2-x}S$ resulting from free carriers, mostly free holes created due to the Cu deficiency.[1, 4] Like metals with high electron density, different compositional copper sulfides except perfect Cu_2S exhibit such plasmonic resonance behavior.[4] Figure 4(d) shows plasmonic NIR spectra of $Cu_{2-x}S$ nanocrystalsat different compositions as reported by Alivisatos et al.[1] The intensity of plasmonic bands can be derived from the Drude model and Mie theory as follows:[1, 4]

$$\omega_p^2 = \frac{4\pi N e^2}{m^*(2\varepsilon_m + \varepsilon_{core})} - \frac{1}{\tau^2} \approx \frac{4\pi N e^2}{m^*(2\varepsilon_m + \varepsilon_{core})}$$

$$K_{ext}(\lambda) = \frac{18 f \varepsilon_m^{3/2} \tau}{\lambda} \frac{(4\pi N e^2)^{1/2}}{m^{*1/2}(2\varepsilon_m + \varepsilon_{core})^{3/2}}$$

where ω_p is the plasmon frequency, N the free carrier concentration, ε as dielectric constant, $k_{ext}(\lambda)$ the extinction coefficient, m^* is the charge carrier effective mass and τ is the average relaxation time. These relationships suggest that plasmon frequency ω_p increases with free carrier concentration ($N^{1/2}$) and extinction coefficient $k_{ext}(\lambda)$ at wavelength λ and also is a function of dielectric constant of the material. An interesting approach to control over the localized surface plasmonic resonance frequency of $Cu_{1.94}S$ was successfully attempted by fabricating dimeric nano heterostructures with ZnS.[111] The strategy was designed with $Cu_{1.94}S$ as plasmonic resonance source, while ZnS acted as tunable dielectric component. Such heteronanostructures exhibited the controllable localized surface plasmonic resonance (LSPR) peak in the range of 1390–680 nm enabling their potential applications in telecommunication.

4.2 Electrical and Thermoelectric Properties

Due to the presence of cationic vacancies in the lattice structure, copper sulfides, $Cu_{2-x}S$ are considered as p-type semiconductors. The close packing, specifically in Cu_2S and $Cu_{1.94}S$ with short Cu-Cu distance like metallic Cu-Cu bonding as well as short Cu-S distance account for their high electrical conductivity.[112] Such a situation converts the material into semimetallic character when attaining the critical temperature of 1.6 K.[113] Owing to high electrical conductivity and low thermal conductivity, copper sulfides are potentially used as excellent thermoelectric materials. However, very limited work has been done on analyzing the electrical properties of copper sulfides particularly in nanodimensional form. According to earlier literature, highly dense $Cu_{2-x}S$ bulks show high thermoelectric performance with Figure of merit (*zT)* value of 1.9 at 970 K.[114] Li et al.[115] prepared $KCu_{7-x}S_4$ nanowires by introducing K^+ into Cu_7S_4 lattice without compromising electrical conductivity. They found that $KCu_{7-x}S_4$ nanowires exhibit efficient thermoelectric property due to the increased Cu deficiency in the lattice and generation of numerous grain boundaries in comparison to pristine Cu_7S_4 nanostructure. However, there exists plenty of scope to investigate the thermoelectric property of different phases of copper sulfides.

5. Applications of Nanostructured Copper Sulfides

5.1 Photocatalysis

Considering the strong absorption in the visible range and stability over a wide range of pH, copper sulfide nanostructures are extensively used in photocatalytic decomposition of various organic pollutants [4, 116-119] This versatility makes copper sulfide nanostructures as replacement to most widely used TiO_2 photocatalyst due to it

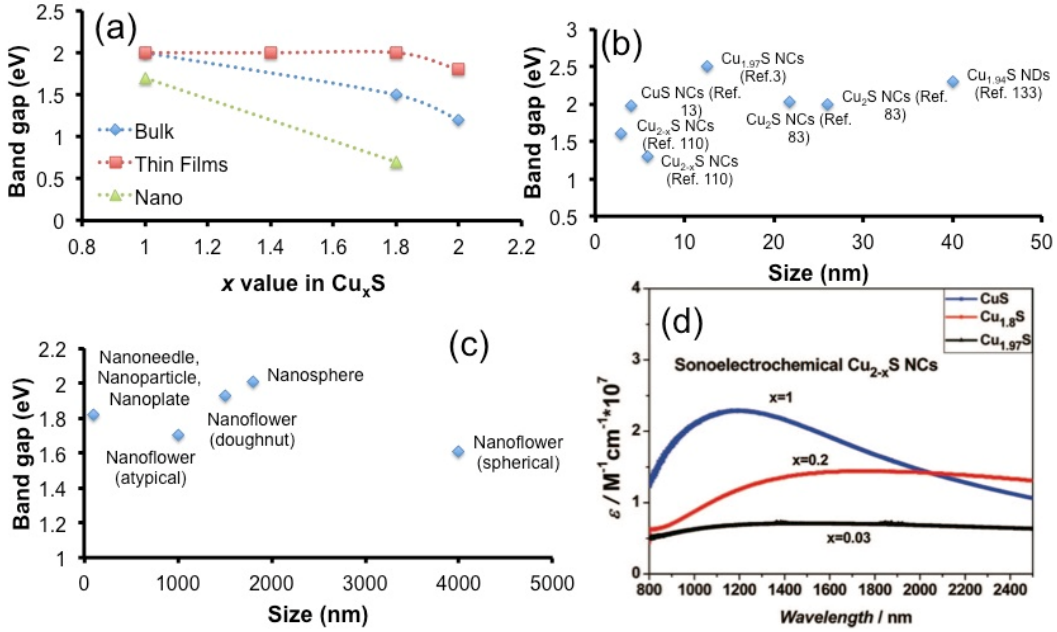

Figure 4: (a-c) Band gap dependence of copper sulfides with composition, size and shape of nanostructures: (a) Band gap as a function of compositions (data sources for bulk: ref. 1; thin films: ref. 9; nano: ref. 55), (b) Band gap as a function of size of nanocrystals or nanodisks (NCs/NDs), and (c) Band gap as a function of shapes of CuS nanostructures (data source: ref. 56); (d) NIR spectra of $Cu_{2-x}S$ NCs with different compositions synthesized by the sonoelectrochemical method. Reprinted with permission from ref. 1. Copyright 2009 American Chemical Society.

limited absorption in the UV range.[56] Therefore, performance of photocatalytic activity of different nanostructures of copper sulfides in presence of different dyes, e.g., methylene blue (MB), Rhodamin B (RhB) etc have extensively been investigated.[55, 56, 117, 120, 121] Fig. 5a describes the mechanism of dye degradation taking place on the surface of copper sulfide nanostructure. Like other semiconducting photocatalysts, copper sulfide nanostructure absorbs visible light and generates e^--h^+ pair in the conduction and valence bands, respectively followed by successful charge transfer to the surface of the nanostructure to react with oxidants and reductants, respectively. Equation (1-6) describe series of chemical reactions taking place between copper sulfide with oxidants and reductants.[56] Subsequently, the superoxide ions ($\cdot O^{2-}$) and ·OH radicals decompose the organic pollutants.

$CuS + h\nu \rightarrow h^+(CuS) + e^-(CuS)$ (1)

$H_2O \rightarrow H^+ + OH^-$ (2)

$e^-(CuS) + O_2 \rightarrow \cdot O_2^-$ (3)

$e^-(CuS) + H_2O_2 \rightarrow \cdot OH + OH^-$ (4)

$h^+(CuS) + OH^- \rightarrow \cdot OH$ (5)

Organic pollutant + $\cdot OH + \cdot O_2^- \rightarrow$ degradation products (6)

Zhang et al.[56] investigated photocatalytic performance of various CuS nanostructures (nanoflowers, dough-nut-shaped nanospheres, dense nanospheres, mixtures of nanoneedles, nanoparticles, and nanoplates) with their band gaps lying in the range of 1.61 -2.01 eV in RhB. Monodispersed CuS microflowers also exhibited excellent photocatalytic activity towards the degradation of MB.[117] Srivastava and coworker[121] observed that CuS nanoparticles degrades MB to ~90% in 90 min and also exhibited excellent reusability. Geng and his co-workers[14] fabricated various controlled architectural ball-flower shaped CuS structures and observed better photocatalytic performance of CuS structure compared to Degussa P25 powders in UV light due to their high surface area. Hierarchical CuS flowers assembled by pure CuS nanosheets (Thicknes: 20 nm) are also found to be very promising photocatalysts with excellent recyclability in photodegradation of MB, RhB or both of them in presence of H_2O_2 under light irradiation.[120] It is noted that presence of H_2O_2 and the visible light are most effective in the fast degradation of dyes due to their synergistic effect as shown in Fig. 5(b).[55] A very fast degradation rate of RhB reaching 98% degradation in 15 min was observed for the mixture of CuS and Cu_7S_4 with flake-like nanostructures in compared to pure CuS and Cu_9S_5.[55] On a different note, there are few reports on CuS nanostructures exhibiting its catalytic activity in presence of H_2O_2 and interestingly in absence of light.[59, 122, 123] The degradation of dyes under dark is attributed to the formation of ·OH radicals in the chemical reaction between CuS and H_2O_2 as described below:[122, 123]

$Cu^{2+} + H_2O_2 \rightarrow H^+ + CuOOH^+$ (7)

$CuOOH^+ \rightarrow HOO^- + Cu^+$ (8)

$Cu^+ + H_2O_2 \rightarrow Cu^{2+} + OH^- + \cdot OH$ (9)

RH (organic dye) + $\cdot OH \rightarrow R^- + H_2O$ (10)

Several attempts have also been made in designing hetero nanostructures to improvise the photocatalytic performances of copper sulfide nanostructures.[122, 124-128] Park and his group[124] synthesized Au-Cu_2S core-shell nanocrystals by solvothermal method and observed ~ 2.5 times enhanced photocatalytic activity under visible light in MB as well as RhB degradation. Such hybrid nanostructures of copper sulfide enhanced performances due to their synergistic effects in compared to the pristine component.

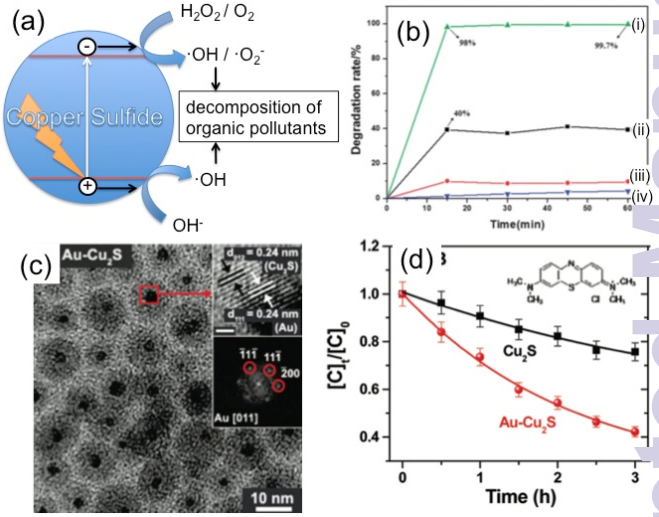

Figure 5: (a) Schematic representation of photocatalytic decomposition of organic pollutants on the surface of copper sulfide nanocrystals; (b) Catalytic performances of CuS nanostructures under different conditions on the degradation rate of RhB (i) in presence of H_2O_2 under visible light; (ii) in presence of H_2O_2 in dark; (iii) without H2O2 under visible light; (iv) only with H_2O_2 without the CuS catalyst in visible light. Reprinted with permission from ref. 55 . Copyright 2013 Royal Society of Chemistry. (c) Au-Cu_2S core-shell nanostructures (inserts: lattice resolved images and FFTED patterns for the Cu_2S and Au) and (d) Comparison between pristine Cu_2S and Au-Cu_2S nanocrystals on photocatalytic degradation of RhB under visible light irradiation. Reprinted with permission from ref. 124. Copyright 2010 American Chemical Society.

5.2 Solar Cells

Copper sulfides attracted lot of attention in solar cells due to their ability to act as light absorbing layer in solar cells.[129] Though, CdS/Cu_2S junction in 1980s exhibited 10% efficiency in solar cell,[130, 131] its scope in solar cell is limited due to diffusion of Cu^+ ions in the CdS layer.[131] Additionally, poor electrical conductivity of $Cu_{2-x}S$ results in high probability of e^--h^+ recombination affecting the overall efficiency of solar cells.[131] These drawbacks has been overcome by using single crystalline copper sulfide nanocrystals[15, 132, 133] or replacing CdS layer by metal oxides, such as TiO_2[134] or ZnO[135]. Alivisatos and his group[15] fabricated the photovoltaic devices composed of CdS/Cu_2S junctions on a conventional glass as well as flexible plastic substrate imparting photo conversion efficiency of 1.6%. Bera et al.[136] studied the current tunneling effect along with the density of states (DOS) spectra in individual nanorods designed as Cu_2S/CdS (*p-n*) or Cu_2S/CdS/Cu_2S (*p-n-p*) heterojunctions to determine the band edges across the junction. It is also reported that Cu_2S/CdS coaxial nanowire showed enhanced performance in photovoltaic devices due to Piezo-phototronics effect.[132] Yang and his research group[137] fabricated single crystalline CdS/Cu_2S core-shell nanowires as an effective *p-n* junction to separate the generated charge carriers and minimize their recombination. The single

crystalline nature of materials demonstrates presence of very few interface defects to account for excellent V_{OC}, FF and an efficiency of 5.4%. The application of hybrid CuS nanotubes–ITO schottky junctions in photovoltaic devices exhibited an efficiency of 1.46%.[99] Further, use of nanocomposites of Cu_2S with MWCNTs in photovoltaic devices has also been reported by elsewhere.[16] As an extended solar cell application, Cu_2S has also been employed in the fabrication of quantum dot sensitized (QDSSC) or dye sensitized solar cells (DSSC).[138-141] It is well-blushed fact that noble metals, such as Pt, Au are widely accepted as counter electrodes in the TiO_2 based QDSSCs and DSSCs. However, the chemisorption of electrolyte on metal catalysts causes high over potential leading to low fill factor. Therefore, Cu_2S has been effectively used as counter electrode due to their higher electrocatalytic activity in reducing S_n^{2-} to nS^{2-} and decreasing charge transfer resistance as well as sheet resistance of counter electrode.[138] Jiang et al.[138] designed counter electrode composed of a coaxial nanowire arrays of ITO as the core and Cu_2S as the sheath against the CdS sensitized TiO_2 (Degussa) layer as photoanode. Such an arrangement in QDSSC leads to a stable efficiency up to 4.06%.

5.3 Energy Storage Devices

Recently, nanostructured materials are being widely used in different energy storage devices, such as lithium ion rechargeable batteries (LIB), supercapacitors etc.[142] In this regard, transition metal chalcogenides are widely accepted as cathode material due to their higher potential versus lithium.[23] Based on the bonding between transition metals and chalcogens, potential range of transition metal chalcogenides can be tuned between 0 to 3.5 V.[143] Among various metal chalcogenides, copper sulfide nanostructures are considered to be efficient cathode materials in lithium ion rechargeable batteries due to high lithium activity, high theoretical capacity, high abundant and low cost.[18, 144] The reactivity of Li/CuS system can be represented as follows:[144]

$$2CuS + 2e^- + 2Li^+ \Leftrightarrow Cu_2S + Li_2S \quad (11)$$

$$Cu_2S + 2e^- + 2Li^+ \Leftrightarrow 2Cu + Li_2S \quad (12)$$

The reversibility of the reactions leads to the good cyclability and high battery performances. 1D nanostructures has also drawn much attention due to directional electronic transportation, high surface area and accommodation of mechanical stress during Li^+ ion insertion and removal process.[142] Lai et al.[18] fabricated Cu_2S nanowire arrays on to the conductive Cu-substrate and used as cathode material in LIB. The electrode showed good capacitive performance of 230 $mAh.g^{-1}$ at high rate of 2C with great cyclic stability up to 100 cycles along with capacity retention value of 96%. Guery and his co-workers[17] synthesized single crystalline CuS thin films containing flake-like structure by electrodeposition technique in ionic liquid media and examined their performance as positive electrode in LIB. Though, electrode initially showed discharge capacity value of 350 $mAhg^{-1}$, confronted capacity fading with capacity retention value of 54% up to 20 cycles. Among different nanostructures, core-shell nanostructure exhibit better LIB performance as the inner hollow space accommodates the strain generated during Li^+ intercalation/deintercalaction process.[145] Another interesting work involved fabrication of Cu_xS/Cu nanotubes by a two-step solvothermal process.[146] It showed excellent Li-storage ability, as the metallic Cu helped in enhancing electron transportation kinetics through the nanotube wall leading high specific capacities as well as high current densities.

A few reports are also available on 1D nanostructured copper sulfide directly grown on to the conductive substrate to facilitate the electronic transportation further through the nanostructure avoiding any loss of electrons to the current collector leading better performance as electrode.[68, 142, 147] Therefore, Hsu et al.[147] fabricated CuS nanowires arrays on Cu-foil, whereas Lou and co-workers[68] designed ultrafine CuS nanoneedles supported on a CNT conductive backbone. Such hybrid nanocomposites exhibit high capacitance value of 100 g^{-1} with excellent cycling stability up to 1000 cycles.

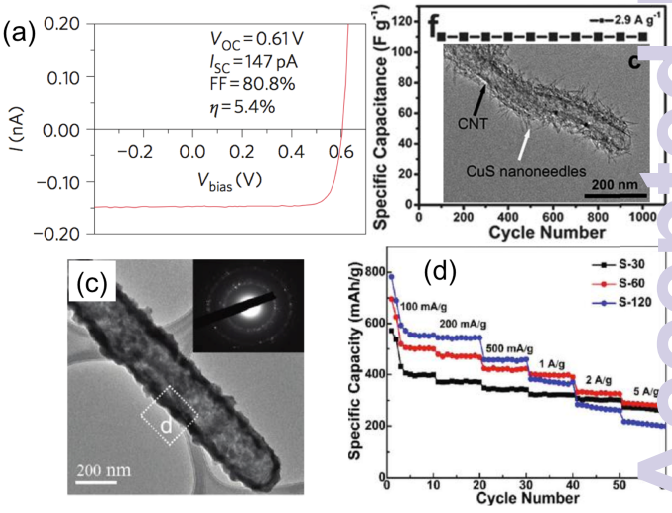

Figure 6: (a) I–V characteristic of a CdS-Cu_2S core–shell nanowire photovoltaic cel under 1 sun (AM 1.5G) illumination. Reprinted with permission from ref. 137. Copyright 2011 Nature Publishing Group. (b) Cycling performance of ultrafine CuS on CNT backbone as supercapacitor at a current density 2.9 A g-1. Reprinted with permission from ref. 68. Copyright 2012 Royal Society of Chemistry. (c) TEM image of CuxS/Cu nanotube (inset: corresponding SAED pattern) and (d) cycling performance of the CuxS/Cu samples in LIB at various C rates. Reprinted with permission from ref. 146. Copyright 2012 American Chemical Society.

5.4 Biomedical Applications

A detailed discussion on biomedical applications of nanostructured CuS has recently been reviewed by Goel et al.[148] CuS has invariably been used for both *in vitro* as well as *in vivo* biological applications due to the non-toxic nature.[18-150] As *in vitro* applications, CuS nanoparticles are extensively used as biosensor for DNA detection, food analysis, bioreactor monitoring etc. Usually, the detection of DNA is carried out by chemiluminescence assays based on the luminescence of enzymes or metal (Au, Ag etc.) attached to the DNA.[148] However, due to the poor stability as well as low detection sensitivity of metals and enzymes, CuS in nanoscale form has been used as an alternative stable material for this purpose.[149, 150]

In biomedical science, detection of glucose level is very important to diagnose many diseases, like diabetes. Though, enzymatic biosensors were extensively used for this purpose, recent advent of nanomaterials with high conductivity

overshadowed the use of relatively less stable enzymes.[148] In comparison to expensive noble metals, low-cost CuS nanomaterials mostly in the nanotubular form with metal-like conductivity were used efficiently used as non-enzymatic biosensors.[16, 63, 85, 97] Further, enhanced glucose sensitivity can also be achieved by hybrid Cu_2S-MWCNT material as reported by elsewhere.[16, 151] Such enhanced activity has been attributed to the synergistic effect of catalytic property of Cu_2S and increased electrical conductivity due to the presence of MWCNT.

The optical activity of copper sulfide in the NIR region (typically in the range of 700–1065 nm) was also used in drug delivery system by photothermal ablation technique for the treatment of tumors.[20, 152-154] Hollow copper sulfide nanoparticles exhibit intense photothermal coupling effects allowing rapid heating and instantaneous heat conduction on absorbing nanosecond-pulsed NIR laser.[152] The phenomena were effectively used as the transdermal delivery system and the changing the power of NIR laser can easily control the depth of skin perforation. Guo et al.[153] carried out a comparative study on photothermal therapy of cancer by hollow CuS nanoparticles and hollow Au nanoparticles with comparable size of nanoparticles. They injected the surface modified nanoparticles (hollow CuS and hollow Au) by polyethylene glycol in a comparative dose and found effective photothermal therapy of CuS over Au nanoparticles due to its non-toxic and biodegradable nature. The fabrication of flower-like CuS superstructures enhances the absorption capability in the NIR region exhibiting almost 50% improvement photothermal conversion efficiency.[20] Feng and coworkers[155] investigated the *in vitro* and *in vivo* toxicity of CuS nanoplates using various cell lines (HeLa, KB, HUVEC and RAW 264.7). They observed no visible toxicity of CuS nanoplates for *in vitro* experiments against HeLa, KB and RAW 264.7 cells up to 100 µg/ml dose. *In vivo* experiments show 7.7 mg/kg CuS nanoplates has no toxic effect on mice. However, biodistribution of CuS nanoplates observed in lungs, spleen and liver due to reticuloendothelial system (RES). Such informations are significant for designing the therapeutic applications of copper sulfide nanostructures.

6. Outlook and Conclusion

Copper sulfides with different cationic vacancies in their crystal lattices exhibit a series of phases with tunable optical and electrical properties. The absorption band of copper sulfide in NIR region accounts for plasmonic effect due to the presence of charge carriers. This is attributed to different compositions and vacancies created in the crystal structures. The crystal packing of $Cu_{2-x}S$ with different x values further exhibit semimetallic behavior. Interestingly, copper sulfides in nanoscale dimension with controlled size and shape opened further a new addition. Accordingly, several synthetic procedures have been employed for designing different nanostructures and in fabrication of hetronanostructures. The wide variations in their compositions, crystal packing and tunable properties make them flexible for many multifaceted applications in many fields. As an effective photocatalyst, nanostructured pristine $Cu_{2-x}S$ and hybrid materials with proper band gap engineering are used for the degradation of organic pollutant. The nanoheterojunctions of copper sulfides with other materials are used in the designing and fabrication of photovoltaic solar cells to minimize the loss of charge carriers generated by light absorption and to attain high photoconversion efficiency. In this regard, fabrication of nanohybrid materials of copper sulfides with conductive CNTs, CNFs or their deposition on conductive substrates, such as ITO coated glass, Cu or Al substrates are found to be very effective approach. Nanostructured $Cu_{2-x}S$ has also been used in lithium ion rechargeable batteries due to high lithium activity and high theoretical capacity. The interesting optical properties as well as the non-toxic nature further allow them to use in different biomedical applications as well.

References

1 Y. X. Zhao, H. C. Pan, Y. B. Lou, X. F. Qiu, J. J. Zhu and C. Burda, *J. Am. Chem. Soc.*, 2009, 131, 4253-4261.
2 P. Lukashev, W. R. L. Lambrecht, T. Kotani and M. v. Schilfgaarde, *Phys. Rev. B*, 2007, 76, 195202.
3 I. Kriegel, J. Rodriguez-Fernandez, E. Da Como, A. A. Lutich, M. Szeifert and J. Feldmann, *Chem Mater*, 2011, 23, 1830-1834.
4 Y. X. Zhao and C. Burda, *Energ Environ Sci*, 2012, 5, 5564-5576.
5 J. Kolny-Olesiak, *Energ Environ Sci*, 2014, DOI: 10.1039/C4CE00674G.
6 E. J. Silvester, F. Grieser, B. A. Sexton and T. W. Healy, *Langmuir*, 1991, 7, 2917-2922.
7 L. G. Liu, H. Z. Zhong, Z. L. Bai, T. Zhang, W. P. Fu, L. J. Shi, H. Y. Xie, L. G. Deng and B. S. Zou, *Chem Mater*, 2013, 25, 4828-4834.
8 Y. Y. Kim and D. Walsh, *Nanoscale*, 2010, 2, 240-247.
9 I. Grozdanov and M. Najdoski, *J. Solid Stat. Chem.*, 1995, 114, 469-475.
10 F. Di Benedetto, M. Borgheresi, A. Caneschi, G. Chastanet, C. Cipriani, D. Gatteschi, G. Pratesi, M. Romanelli and R. Sessoli, *Eur J Mineral*, 2006, 18, 283-287.
11 X. L. Yu, C. B. Cao, H. S. Zhu, Q. S. Li, C. L. Liu and Q. H. Gong, *Adv Funct Mater*, 2007, 17, 1397-1401.
12 Y. B. Lou, A. C. S. Samia, J. Cowen, K. Banger, X. B. Chen, H. Lee and C. Burda, *Phys. Chem. Chem. Phys.*, 2003, 5, 1091-1095.
13 M. Tanveer, C. B. Cao, Z. Ali, I. Aslam, F. Idrees, W. S. Khan, F. K. But, M. Tahir and N. Mahmood, *CrystEngComm*, 2014, 16, 5290-5300.
14 Z. G. Cheng, S. Z. Wang, Q. Wang and B. Y. Geng, *CrystEngComm*, 2010, 12, 144-149.
15 Y. Wu, C. Wadia, W. L. Ma, B. Sadtler and A. P. Alivisatos, *Nano Lett*, 2008, 8, 2551-2555.
16 H. Lee, S. W. Yoon, E. J. Kim and J. Park, *Nano Lett*, 2007, 7, 778-784.
17 Y. H. Chen, C. Davoisne, J. M. Tarascon and C. Guery, *J Mater Chem*, 2012, 22, 5295-5299.
18 C. H. Lai, K. W. Huang, J. H. Cheng, C. Y. Lee, B. J. Hwang and L. J. Chen, *J Mater Chem*, 2010, 20, 6638-6645.
19 X. Y. Bu, D. Zhou, J. Li, X. Zhang, K. Zhang, H. Zhang and B. Yang, *Langmuir*, 2014, 30, 1416-1423.
20 Q. W. Tian, M. H. Tang, Y. G. Sun, R. J. Zou, Z. G. Chen, M. F. Zhu, S. P. Yang, J. L. Wang, J. H. Wang and J. Q. Hu, *Adv Mater*, 2011, 23, 3542-3547.

21 G. Ku, M. Zhou, S. L. Song, Q. Huang, J. Hazle and C. Li, *ACS Nano*, 2012, 6, 7489-7496.
22 C. Burda, X. B. Chen, R. Narayanan and M. A. El-Sayed, *Chem Rev*, 2005, 105, 1025-1102.
23 M. R. Gao, Y. F. Xu, J. Jiang and S. H. Yu, *Chem Soc Rev*, 2013, 42, 2986-3017.
24 M. Xu, H. Y. Wu, P. M. Da, D. Y. Zhao and G. F. Zheng, *Nanoscale*, 2012, 4, 1794-1799.
25 P. Leidinger, R. Popescu, D. Gerthsen, H. Lunsdorf and C. Feldmann, *Nanoscale*, 2011, 3, 2544-2551.
26 Q. Y. Lu, F. Gao and D. Y. Zhao, *Nano Lett*, 2002, 2, 725-728.
27 R. H. Kore, J. S. Kulkami and S. K. Haram, *Chem Mater*, 2001, 13, 1789-1793.
28 M. Shamsipur, S. M. Pourmortazavi, M. Roushani and S. S. Hajimirsadeghi, *Synth React Inorg M*, 2014, 44, 951-958.
29 H. B. Wu and W. Chen, *Nanoscale*, 2011, 3, 5096-5102.
30 W. J. Lou, M. Chen, X. B. Wang and W. M. Liu, *J Phys Chem C*, 2007, 111, 9658-9663.
31 W. M. Du, X. F. Qian, X. D. Ma, Q. Gong, H. L. Cao and H. Yin, *Chem-Eur J*, 2007, 13, 3241-3247.
32 M. Kruszynska, H. Borchert, A. Bachmatiuk, M. H. Rummeli, B. Buchner, J. Parisi and J. Kolny-Olesiak, *ACS Nano*, 2012, 6, 5889-5896.
33 T. H. Larsen, M. Sigman, A. Ghezelbash, R. C. Doty and B. A. Korgel, *J Am Chem Soc*, 2003, 125, 5638-5639.
34 X. H. Liao, N. Y. Chen, S. Xu, S. B. Yang and J. J. Zhu, *J Cryst Growth*, 2003, 252, 593-598.
35 K. V. Singh, A. A. Martinez-Morales, G. T. S. Andavan, K. N. Bozhilov and M. Ozkan, *Chem Mater*, 2007, 19, 2446-2454.
36 M. T. Mayer, Z. I. Simpson, S. Zhou and D. W. Wang, *Chem Mater*, 2011, 23, 5045-5051.
37 Q. F. Han, S. S. Sun, J. S. Li and X. Wang, *Nanotechnol*, 2011, 22.
38 X. Y. Wang, Z. Fang and X. Lin, *J Nanopart Res*, 2009, 11, 731-736.
39 Y. N. Xia, P. D. Yang, Y. G. Sun, Y. Y. Wu, B. Mayers, B. Gates, Y. D. Yin, F. Kim and Y. Q. Yan, *Adv Mater*, 2003, 15, 353-389.
40 L. X. Yi, Y. Y. Liu, N. L. Yang, Z. Y. Tang, H. J. Zhao, G. H. Ma, Z. G. Su and D. Wang, *Energ Environ Sci*, 2013, 6, 835-840.
41 J. Y. Chang and C. Y. Cheng, *Chem Commun.*, 2011, 47, 9089-9091.
42 L. X. Yi, A. W. Tang, M. Niu, W. Han, Y. B. Hou and M. Y. Gao, *CrystEngComm*, 2010, 12, 4124-4130.
43 S. K. Han, M. Gong, H. B. Yao, Z. M. Wang and S. H. Yu, *Angew Chem Int Ed*, 2012, 51, 6365-6368.
44 T. Y. Zhai, X. S. Fang, L. Li, Y. Bando and D. Golberg, *Nanoscale*, 2010, 2, 168-187.
45 S. Kar and S. Chaudhuri, *Synth React Inorg M*, 2006, 36, 289-312.
46 J. H. Han, S. Lee and J. Cheon, *Chem Soc Rev*, 2013, 42, 2581-2591.
47 S. V. Kershaw, A. S. Susha and A. L. Rogach, *Chem Soc Rev*, 2013, 42, 3033-3087.
48 R. J. Goble, *Can Mineral*, 1985, 23, 61-76.
49 Y. Xie, A. Riedinger, M. Prato, A. Casu, A. Genovese, P. Guardia, S. Sottini, C. Sangregorio, K. Miszta, S. Ghosh, T. Pellegrino and L. Manna, *J Am Chem Soc*, 2013, 135, 17630-17637.
50 Q. Xu, B. Huang, Y. F. Zhao, Y. F. Yan, R. Noufi and S. H. Wei, *Appl Phys Lett*, 2012, 100.
51 P. Nørby, S. Johnsen and B. B. Iversen, *ACS Nano*, 2014, 8, 4295-4303.
52 W. P. Lim, C. T. Wong, S. L. Ang, H. Y. Low and W. S. Chin, *Chem Mater*, 2006, 18, 6170-6177.
53 S. Cassaignon, S. Sanchez, J. F. Guillemoles, J. Vedel and H. G. Meier, *J Electrochem Soc*, 1999, 146, 4666-4671.
54 B. R. Jia, M. L. Qin, X. Z. Jiang, Z. L. Zhang, L. Zhang, Y. Liu and X. H. Qu, *J Nanopart Res*, 2013, 15.
55 M. R. Wang, F. Xie, W. J. Li, M. F. Chen and Y. Zhao, *J Mater Chem A*, 2013, 1, 8616-8621.
56 Y. Q. Zhang, B. P. Zhang, Z. H. Ge, L. F. Zhu and Y. Li, *Eur J Inorg Chem*, 2014, 2014, 2368-2375.
57 Y. L. Auyoong, P. L. Yap, X. Huang and S. B. Abd Hamid, *Chem Cent J*, 2013, 7.
58 S. K. Goswami, J. Kim, K. Hong, E. Oh, Y. Yang and D. Yu, *Mater Lett*, 2014, 133, 132-134.
59 J. Kundu and D. Pradhan, *ACS Appl Mater Interf*, 2014, 6, 1823-1834.
60 A. M. Qin, Y. P. Fang, H. D. Ou, H. Q. Liu and C. Y. Su, *Cryst Growth Des*, 2005, 5, 855-860.
61 P. Roy and S. K. Srivastava, *Cryst Growth Des*, 2006, 6, 1921-1926.
62 Z. Zhuang, Q. Peng, B. Zhang and Y. Li, *J Am Chem Soc*, 2008, 130, 10482.
63 X. J. Zhang, G. F. Wang, A. X. Gu, Y. Wei and B. Fang, *Chem Commun.*, 2008, DOI: Doi 10.1039/B814725f, 5945-5947.
64 S. He, G.-S. Wang, C. Lu, J. Liu, B. Wen, H. Liu, L. Guo and M. S. Cao, *J Mater Chem A*, 2013, 1, 4685.
65 P. Roy and S. K. Srivastava, *J Nanosci Nanotechnol*, 2008, 1523-1527.
66 S. Gorai, D. Ganguli and S. Chaudhuri, *Cryst Growth Des*, 2005, 5, 875–877.
67 G. Y. Chen, B. Deng, G. B. Cai, W. F. Dong, W. X. Zhang and A. W. Xu, *Cryst Growth Des*, 2008, 8, 2137-2143.
68 T. Zhu, B. Y. Xia, L. Zhou and X. W. Lou, *J Mater Chem*, 2012, 22, 7851-7855.
69 G. B. Jung, Y. Myung, Y. J. Cho, Y. J. Sohn, D. M. Jang, H. S. Kim, C. W. Lee, J. Park, I. Maeng, J. H. Son and C. Kang, *J Phys Chem C*, 2010, 114, 11258-11265.
70 Z. Y. Zhan, C. Liu, L. X. Zheng, G. Z. Sun, B. S. Li and Q. Zhang, *Phys Chem Chem Phys*, 2011, 13, 20471-20475.
71 Y. Xie, L. Carbone, C. Nobile, V. Grillo, S. D'Agostino, F. Della Sala, C. Giannini, D. Altamura, C. Oelsner, C. Kryschi and P. D. Cozzoli, *ACS Nano*, 2013, 7, 7352-7369.
72 P. L. Saldanha, R. Brescia, M. Prato, H. B. Li, M. Povia, L. Manna and V. Lesnyak, *Chem Mater*, 2014, 26, 1442-1449.
73 C. D. Donega, P. Liljeroth and D. Vanmaekelbergh, *Small*, 2005, 1, 1152-1162.
74 C. B. Murray, D. J. Norris and M. G. Bawendi, *J Am Chem Soc*, 1993, 115, 8706–8715.
75 A. Ghezelbash and B. A. Korgel, *Langmuir*, 2005, 21, 9451-9456.
76 N. J. Freymeyer, P. D. Cunningham, E. C. Jones, B. J. Golden, A. M. Wiltrout and K. E. Plass, *Cryst Growth Des*, 2013, 13, 4059-4065.
77 A. W. Tang, S. C. Qu, K. Li, Y. B. Hou, F. Teng, J. Cao, Y. S. Wang and Z. G. Wang, *Nanotechnology*, 2010, 21.
78 G. X. Ma, Y. L. Zhou, X. Y. Li, K. Sun, S. Q. Liu, J. Q. Hu and N. A. Kotov, *ACS Nano*, 2013, 7, 9010-9018.
79 W. Han, L. X. Yi, N. Zhao, A. W. Tang, M. Y. Gao and Z. Y. Tang, *J Am Chem Soc*, 2008, 130, 13152-13161.
80 F. Huang, X. Wang, J. Xu, D. Chen and Y. Wang, *J. Mater. Chem.*, 2012, 22, 22614.
81 M. B. Sigman, A. Ghezelbash, T. Hanrath, A. E. Saunders, F. Lee and B. A. Korgel, *J Am Chem Soc*, 2003, 125, 16050-16057.
82 L. Chen, Y. B. Chen and L. M. Wu, *J Am Chem Soc*, 2004, 126, 16334-16335.
83 Y. B. Chen, L. Chen and L. M. Wu, *Chem-Eur J*, 2008, 14, 11069-11075.
84 I. Jen-La Plante, T. W. Zeid, P. D. Yang and T. Mokari, *J Mater Chem*, 2010, 20, 6612-6617.
85 J. Liu and D. F. Xue, *J Mater Chem*, 2011, 21, 223-228.
86 P. Kar, S. Farsinezhad, X. J. Zhang and K. Shankar, *Nanoscale*, 2014, 6, 14305-14318.
87 Y. J. Zhu and F. Chen, *Chem Rev*, 2014, 114, 6462-6555.

88 T. Thongtem, A. Phuruangrat and S. Thongtem, *Mater Lett*, 2010, 64, 136-139.
89 C. F. Mu, Q. Z. Yao, X. F. Qu, G. T. Zhou, M. L. Li and S. Q. Fu, *Colloid Surface A*, 2010, 371, 14-21.
90 M. Nafees, S. Ali, K. Rasheed and S. Idrees, *Appl. Nanosci.*, 2012, 2, 157–162.
91 M. D. Xin, K. W. Li and H. Wang, *Appl Surf Sci*, 2009, 256, 1436-1442.
92 F. F. Wang, H. Dong, J. L. Pan, J. J. Li, Q. Li and D. S. Xu, *J Phys Chem C*, 2014, 118, 19589-19598.
93 S. S. Dhasade, J. S. Patil, J. H. Kim, S. H. Han, M. C. Rath and V. J. Fulari, *Mater Chem Phys*, 2012, 137, 353-358.
94 A. Ghahremaninezhad, E. Asselin and D. G. Dixon, *Electrochem Commun*, 2011, 13, 12-15.
95 P. Roy, K. Mondal and S. K. Srivastava, *Cryst Growth Des*, 2008, 8, 1530-1534.
96 J. Mao, Q. Shu, Y. Wen, H. Yuan, D. Xiao and M. M. F. Choi, *Cryst Growth Des*, 2009, 9, 2546-2548.
97 Qian, J. F. Mao, X. Q. Tian, H. Y. Yuan and D. Xiao, *Sensor Actuat B-Chem*, 2013, 176, 952-959.
98 L. Qian, X. Q. Tian, L. Yang, J. F. Mao, H. Y. Yuan and D. Xiao, *RSC Adv*, 2013, 3, 1703-1708.
99 C. Y. Wu, Z. H. Zhang, Y. L. Wu, P. Lv, B. A. Nie, L. B. Luo, L. Wang, J. G. Hu and J. S. Jie, *Nanotechnology*, 2013, 24.
100 C. Y. Wu, S. H. Yu, S. F. Chen, G. N. Liu and B. H. Liu, *J Mater Chem*, 2006, 16, 3326-3331.
101 X. L. Liu and Y. J. Zhu, *Mater Lett*, 2011, 65, 1089-1091.
102 J. Xu, W. X. Zhang, Z. H. Yang and S. H. Yang, *Inorg Chem*, 2008, 47, 699-704.
103 J. R. Huang, Y. Y. Wang, C. P. Gu and M. H. Zhai, *Mater Lett*, 2013, 99, 31-34.
104 Y. H. Tseng, Y. He, S. Lakshmanan, C. Yang, W. Chen and L. Que, *Nanotechnology*, 2012, 23.
105 Y. He, S. Vasiraju and L. Que, *RSC Adv*, 2014, 4, 2433-2439.
106 J. Xu, Y. B. Tang, X. Chen, C. Y. Luan, W. F. Zhang, J. A. Zapien, W. J. Zhang, H. L. Kwong, X. M. Meng, S. T. Lee and C. S. Lee, *Adv Funct Mater*, 2010, 20, 4190-4195.
107 M. T. S. Nair, L. Guerrero and P. K. Nair, *Semicond Sci Tech*, 1998, 13, 1164-1169.
108 T. S. Moss, *Proc. Phys. Soc. B*, 1954, 67, 775-782.
109 E. Burstein, *Phys. Rev. B*, 1954, 93, 632-633.
110 J. M. Luther, P. K. Jain, T. Ewers and A. P. Alivisatos, *Nat Mater*, 2011, 10, 361-366.
111 F. Huang, X. Wang, J. Xu, D. Chen and Y. Wang, *J Mater Chem*, 2012, 22, 22614.
112 A. V. Naumov, V. N. Semenov, A. N. Lukin and E. G. Goncharov, *Inorg Mater*, 2002, 38, 343-346.
113 F. D. Benedetto, M. Borgheresi, A. Caneschi, G. Chastanet, C. Cipriani, D. Gatteschi, G. Pratesi, M. Romanelli And R. Sessoli, *Eur. J. Mineral.*, 2006, 18, 283.
114 L. Zhao, X. Wang, F. Y. Fei, J. Wang, Z. Cheng, S. Dou, J. Wang and G. J. Snyder, *J Mater Chem A*, 2015, 3, 9432-9437.
115 X. Y. Li, C. G. Hu, X. L. Kang, Q. Len, Y. Xi, K. Y. Zhang and H. Liu, *J Mater Chem A*, 2013, 1, 13721-13726.
116 A. Ghosh and A. Mondal, *Appl Surf Sci*, 2015, 328, 63-70.
117 Z. K. Yang, L. X. Song, Y. Teng and J. Xia, *J Mater Chem A*, 2014, 2, 20004-20009.
118 M. Basu, A. K. Sinha, M. Pradhan, S. Sarkar, Y. Negishi, Govind and T. Pal, *Environ Sci Technol*, 2010, 44, 6313-6318.
119 Z. Hai, J. Huang, H. Remita and J. Chen, *Mater Lett*, 2013, 108, 304.
120 M. Tanveer, C. B. Cao, I. Aslam, Z. Ali, F. Idrees, W. S. Khan, M. Tahir, S. Khalid, G. Nabi and A. Mahmood, *New J Chem*, 2015, 39, 1459-1468.
121 A. K. Sahoo and S. K. Srivastava, *J Nanopart Res*, 2013, 15.
122 L. W. Mi, W. T. Wei, Z. Zheng, Y. Gao, Y. Liu, W. H. Chen and X. X. Guan, *Nanoscale*, 2013, 5, 6589-6598.
123 Q. W. Shu, J. Lan, M. X. Gao, J. Wang and C. Z. Huang, *CrystEngComm*, 2015, 17, 1374-1380.
124 Y. Kim, K. Y. Park, D. M. Jang, Y. M. Song, H. S. Kim, Y. J. Cho, Y. Myung and J. Park, *J Phys Chem C*, 2010, 114, 22141-22146.
125 U. T. D. Thuy, N. Q. Liem, C. M. A. Parlett, G. M. Lalev and K. Wilson, *Catal Commun*, 2014, 44, 62-67.
126 J. E. Macdonald, M. Bar Sadan, L. Houben, I. Popov and U. Banin, *Nat Mater*, 2010, 9, 810-815.
127 K. H. Ji, D. M. Jang, Y. J. Cho, Y. Myung, H. S. Kim, Y. Kim and J. Park, *J Phys Chem C*, 2009, 113, 19966-19972.
128 C. Ratanatawanate, A. Bui, K. Vu and K. J. Balkus, *J Phys Chem C*, 2011, 115, 6175-6180.
129 K. Ramasamy, M. A. Malik, N. Revaprasadu and P. O'Brien, *Chem Mater*, 2013, 25, 3551-3569.
130 J. A. Bragangolo, A. M. Barnett, J. E. Phillips, R. B. Hall, A. Rothwarf and J. D. Meakin, *IEEE Trans. Electron Devices*, 1980, 27, 645.
131 M. Page, O. Niitsoo, Y. Itzhaik, D. Cahen and G. Hodes, *Energ Environ Sci*, 2009, 2, 220-223.
132 C. F. Pan, S. M. Niu, Y. Ding, L. Dong, R. M. Yu, Y. Liu, G. Zhu and Z. L. Wang, *Nano Lett*, 2012, 12, 3302-3307.
133 M. D. Regulacio, C. Ye, S. H. Lim, M. Bosman, L. Polavarapu, W. L. Koh, J. Zhang, Q. H. Xu and M. Y. Han, *J Am Chem Soc*, 2011, 133, 2052-2055.
134 L. Reijnen, B. Meester, A. Goossens and J. Schoonman, *Mat Sci Eng C-Bio S*, 2002, 19, 311-314.
135 M. Burgelman and H. J. Pauwels, *Electron. Lett.*, 1981, 17, 224.
136 A. Bera, S. Dey and A. J. Pal, *Nano Lett*, 2014, 14, 2000-2005.
137 J. Tang, Z. Huo, S. Brittman, H. Gao and P. Yang, *Nat Nanotechnol*, 2011, 6, 568-572.
138 Y. Jiang, X. Zhang, Q. Q. Ge, B. B. Yu, Y. G. Zou, W. J. Jiang, W. G. Song, L. J. Wan and J. S. Hu, *Nano Lett*, 2014, 14, 365-372.
139 Q. Shen, A. Yamada, S. Tamura and T. Toyoda, *Appl Phys Lett*, 2010, 97.
140 Z. Y. Peng, Y. L. Liu, Y. H. Zhao, K. Q. Chen, Y. Q. Cheng and W. Chen, *Electrochim Act*, 2014, 135, 276-283.
141 X. M. Shuai, W. Z. Shen, Z. Y. Hou, S. M. Ke, C. L. Xu and C. Jiang, *Nanoscale Res Lett*, 2014, 9.
142 P. Roy and S. K. Srivastava, *J Mater Chem A*, 2015, 3, 2454-2484.
143 H. Li, P. Balaya and J. Maier, *J Electrochem Soc*, 2004, 151, A1878-A1885.
144 A. Debart, L. Dupont, R. Patrice and J. M. Tarascon, *Solid State Sci*, 2006, 8, 640-651.
145 M. Nagarathinam, K. Saravanan, W. L. Leong, P. Balaya and J. J. Vittal, *Cryst Growth Des*, 2009, 9, 4461-4470.
146 R. Cai, J. Chen, J. X. Zhu, C. Xu, W. Y. Zhang, C. M. Zhang, W. H. Shi, H. T. Tan, D. Yang, H. H. Hng, T. M. Lim and Q. Y. Yan, *J Phys Chem C*, 2012, 116, 12468-12474.
147 Yu-Kuei Hsu, Ying-Chu Chen and Y.-G. Lin, *Electrochim Act*, 2014, 139, 401.
148 S. Goel, F. Chen and W. Cai, *Small*, 2014, 10, 631-645.
149 S. Zhang, H. Zhong and C. Ding, *Anal Chem*, 2008, 80, 7206-7212.
150 C. Ding, H. Zhong and S. Zhang, *Biosens Bioelectron*, 2008, 23, 1314-1318.
151 Y. Myung, D. M. Jang, Y. J. Cho, H. S. Kim, J. Park, J. U. Kim, J. Choi and C. J. Lee, *J Phys Chem C*, 2009, 113, 1251-1259.
152 S. Ramadan, L. R. Guo, Y. J. Li, B. F. Yan and W. Lu, *Small*, 2012, 8, 3143-3150.
153 L. R. Guo, I. Panderi, D. D. Yan, K. Szulak, Y. J. Li, Y. T. Chen, H. Ma, D. B. Niesen, N. Seeram, A. Ahmed, B. F. Yan, D. Pantazatos and W. Lu, *ACS Nano*, 2013, 7, 8780-8793.

154 M. Zhou, R. Zhang, M. A. Huang, W. Lu, S. L. Song, M. P. Melancon, M. Tian, D. Liang and C. Li, *J Am Chem Soc*, 2010, 132, 15351-15358.
155 W. Feng, W. Nie, Y. Cheng, X. Zhou, L. Chen, K. Qiu, Z. Chen, M. Zhu and C. He, *Nanomed Nanotech Biol Med*, 2015, 11, 901-912.